Path-integral Monte Carlo study of crystalline Lennard-Jones systems

M. H. Müser, P. Nielaba, and K. Binder
Institut für Physik, Johannes-Gutenberg-Universität, KoMa 331, D-55099 Mainz, Federal Republic of Germany
(Received 27 July 1994)

The capability of the path-integral Monte Carlo (PIMC) method to describe thermodynamic and structural properties of solids at low temperatures is studied in detail, considering the noble-gas crystals as examples. In order to reduce the systematic limitations due to finite Trotter number and finite particle number we propose a combined Trotter and finite-size scaling. As a special application of the PIMC method we investigate ^{40}Ar at constant volume and in the harmonic approximation. Furthermore, isotope effects in the lattice constant of ^{20}Ne and ^{22}Ne are computed at zero pressure. The obtained results are compared with classical Monte Carlo results and with experimental data.

I. INTRODUCTION

The path-integral Monte Carlo technique (PIMC) is a widely used method in condensed matter physics[1] to compute quantum effects in solids and liquids. Mostly the method is applied to so-called strong quantum systems, in which exchange of particles or tunneling are playing a dominant role, like superfluid helium, proton tunneling, superconductivity, see, e.g., Refs. 2 and 3. Recently the interest has also been focused on weak quantum systems in order to include the nontrivial influence of the quantum nature on thermodynamic and static properties of condensed matter, as seen in dense rare gas systems (solids, liquids, and clusters). Since the interaction of rare gas atoms can be described very accurately by simple model potentials, comparison of computed data with an experimental one can be carried out easily. Examples in the literature are the investigation of quantum effects in solid and liquid ^{4}He,[4] liquid neon,[5,6] inclusion of nonharmonic interactions in the description of crystalline Ar,[7] and the isotope shift in the melting pressure of ^{3}He and ^{4}He.[8,9]

Nevertheless the capabilities and limitations of the PIMC method in describing low temperature behavior of dense Lennard-Jones or related systems have not yet been discussed in detail. However this is necessary if the range of validity of a simulation has to be judged. The factors limiting the accuracy of the standard PIMC algorithm are the finiteness of the Trotter number and finiteness of the particle number. It is standard to apply Trotter scaling to extrapolate to the exact quantum limit, reached at infinite Trotter number. Finite particle numbers and Born–von Karman periodic boundary conditions, as customarily installed in a computer simulation, involve a discretization of phonon spectra. For low frequencies the density of states contains a gap between zero frequency and the lowest mode given by acoustic phonons with wavelength equal to the linear size of the box. Thus if the temperature is smaller than the energy of the lowest energy vibrational excitation in the system, the computer solid freezes completely, although in real solids (we have in mind ideal crystals) there always remain some long-wave excitations which are still thermally excited, leading typically to a specific heat proportional to the third power of temperature. In this sense the number of simulated atoms has to be increased when temperature is lowered in order to avoid such discretization effects. The total number of simulated beads in the PIMC method (equal to particle number times Trotter number), that needs to be taken into account for quantitatively accurate results, thus increases due to increasing particle number and due to increasing Trotter number when temperature is lowered. Keeping in mind that correlation times usually also increase with increasing Trotter number, it is evident that there is a range of temperature, where some properties of the solid can no more be computed accurately.

In this work we propose a low temperature finite-size scaling method for systems where momentum eigenvalues are good quantum numbers, and apply it to an Ar crystal treated in the harmonic approximation (with finite and infinite Trotter numbers), since in this approximation analytical results for given particle number and Trotter number can be evaluated[10] and expensive simulations have not to be carried out explicitly. We show that the application of this low temperature scaling strongly reduces the number of particles to be simulated.

Of course we also examine the quality of the harmonic approximation and compare analytical results with PIMC data computed from the full pair potentials for some selected combinations of the system parameters temperature, system size, and Trotter number.

While the computation of low temperature specific heat of solids turns out to be very expensive in CPU time within the PIMC formalism, there exist some other pure quantum effects, where the application of the PIMC method should be more efficient. One-well known example is the isotope effect in the lattice constant of solid neon, which has been determined experimentally with a high resolution.[11] In comparison to argon, neon has a smaller mass and a smaller atomic radius. Furthermore the potential of neon is not very deep. Due to Heisenberg's uncertainty principle, neon atoms have a relatively strong zero point motion and thus the atoms move into the nonharmonic part of the potential even at low temperature. This in turn leads to a mass dependent lattice

constant. We carry out a PIMC simulation at zero pressure and compare the obtained isotope shift in the lattice constant of ^{20}Ne and ^{22}Ne with experimental data.

II. THE PATH INTEGRAL MONTE CARLO METHOD

A. The NpT ensemble

PIMC techniques are typically used to calculate expectation values of observables in the (N,V,T) ensemble. In order to carry out a PIMC simulation, an approximant for the density matrix has to be formulated, which gives an instruction how to generate a random walk through phase space, respecting the principles of detailed balance. During this walk, approximants for the observables are averaged, yielding the expectation value of the observable in the given approximation.

The so-called primitive form of PIMC has its origin in Feynman's formulation[12] of the canonical partition function $Q(N,V,T)$. Meanwhile there exist better approximants for the density matrix, for a thorough presentation see, e.g., Ref. 13, but for our purposes the primitive algorithm already yielded satisfactory results. One point particle with a mass m is represented by a chain of classical "beads," numbered $t=0,1,...,P$. In the isomorphic classical picture[14] of distinguishable particles every bead interacts within the chain with its next neighbors and interaction between the chains only takes place by beads with the same bead number. The canonical partition function is

$$Q(N,V,T)=\lim_{P\to\infty}\left(\frac{mP}{2\pi\hbar^2\beta}\right)^{dNP/2}\times\int_v d\{\bar{r}\}\exp\left[-\frac{\beta}{P}H_{(P)}(\{\bar{r}\})\right] \tag{1}$$

with

$$H_{(P)}(\{\bar{r}\})=\sum_{i=1}^{N}\sum_{t=1}^{P}\left(t_i^{(t)}+v_i^{(t)}\right), \tag{2a}$$

$$t_i^{(t)}=\frac{mP^2}{2\hbar^2\beta^2}\left(\bar{r}_i^{(t)}-\bar{r}_i^{(t-1)}\right)^2, \tag{2b}$$

$$v_i^{(t)}=\sum_{i<j}v\left(\mid\bar{r}_i^{(t)}-\bar{r}_j^{(t)}\mid\right), \tag{2c}$$

$\{\bar{r}\}$ denotes the complete set of $\bar{r}_i^{(t)}$ being the coordinate of the bead at Trotter index t corresponding to the ith point particle. $\bar{r}_i^{(0)}$ has to be chosen identical with $\bar{r}_i^{(P)}$. In Eq. (2) for simplicity we have specialized to pairwise interaction between the point particles $v(\mid\bar{r}_i^{(t)}-\bar{r}_j^{(t)}\mid)$.

The integration in Eq. (1) is constrained to a fixed d-dimensional volume V. In the case of constant pressure we are interested in the formulation of the isothermal-isobaric partition function $\Delta(N,p,T)$:

$$\Delta(N,p,T)=\int dV e^{-\beta PV}Q(N,V,T)\ . \tag{3}$$

In the following every real vector $\bar{r}_i^{(t)}$ is expressed as $s\bar{r}_{i,0}^{(t)}$, where s has the meaning of a scale variable and the vector $\bar{r}_{i,0}^{(t)}$ is constrained to a reference volume V_0. One configuration is thus characterized by the complete set of the Monte Carlo variables $s,\{\bar{r}_0\}$. If we write the unnormalized probability of one configuration as $\exp\left[-\beta E_{(P)}(s,\{\bar{r}_0\})\right]$ one can write, with Eqs. (1)–(3),

$$E_{(P)}(s,\{\bar{r}_0\})=-k_BT[d(NP+1)-1]\ln(s)+pV_0s^d+H_{(P)}(\{s\bar{r}_0\})+\frac{v_{0,6}^{(\mathrm{cor})}}{s^6}+\frac{v_{0,12}^{(\mathrm{cor})}}{s^{12}}. \tag{4}$$

The terms $v_{0,n}^{(\mathrm{cor})}$ are potential corrections, due to the cutoff in the Lennard-Jones potential and will be discussed in Sec. II B. The Metropolis procedure can now be applied. Thermodynamic functions are expressed in terms of average quantities $[\cdots]_{\mathrm{MC}}$ of the classical system. It is convenient to measure the kinetic energy T_{kin} with an approximant which is diagonal in the coordinate representation[15] [see Eq. (5b)], because the statistical error does not increase with increasing Trotter number P. Pressure p can be computed to test self-consistence and for this purpose it is sufficient to use the straightforward expression[8]

$$V_{\mathrm{pot}}=\lim_{P\to\infty}\frac{1}{P}\left[\sum_{i=1}^{N}\sum_{t=1}^{P}v_i^{(t)}\right]_{\mathrm{MC}}, \tag{5a}$$

$$T_{\mathrm{kin}}=\lim_{P\to\infty}\frac{1}{2P}\left[\sum_{i=1}^{N}\sum_{t=1}^{P}s\bar{r}_{i,0}^{(t)}\frac{\partial}{\partial\left(s\bar{r}_{i,0}^{(t)}\right)}v_i(\{s\bar{r}_0\})\right]_{\mathrm{MC}}, \tag{5b}$$

$$p=\lim_{P\to\infty}\left[\frac{PNk_BT}{s^dV_0}-\frac{1}{ds^dV_0P}\left(\sum_{i=1}^{N}\sum_{t=1}^{P}2s^2t_{0,i}^{(t)}+\sum_{i=1}^{N}\sum_{t=1}^{P}s\frac{\partial}{\partial s}\left[v_i^{(t)}\left(\left\{s\bar{r}_0\right\}\right)+v^{(\mathrm{cor})}(s)\right]\right)\right]_{\mathrm{MC}} \tag{5c}$$

The determination of lattice constant a is trivial:

$$a=a_0\lim_{P\to\infty}[s]_{\mathrm{MC}} \tag{6}$$

with a_0 being the lattice constant of the system with volume V_0. It is worth mentioning that the two sums containing derivatives in Eqs. (5b) and (5c) are not equivalent virial expressions, because of periodic boundary conditions. That is why correction potentials have to be considered in the computation of the pressure, but not in the computation of T_{kin}.

B. Technical details

We consider a system, consisting of N distinguishable point particles with mass m, interacting via a Lennard-Jones potential $v(r_{ij}) = 4\epsilon(\frac{\sigma}{r_{ij}})^6[(\frac{\sigma}{r_{ij}})^6 - 1]$. We choose standard values for neon and argon potentials.[16] Exchange is neglected, since this effect would only be important for Ne if the mass would be smaller than 2 amu.[17] Three-body interactions have been neglected also, because at low pressures they do not play a significant role and their computation is rather expensive in CPU time. In most of the simulations, we put 256 or 500 particles in the box.

Interactions have been taken into account up to the fourth neighboring shell, so that in fcc symmetry one particle interacts with 54 neighboring particles. Their contribution is about 90% of the total energy or of the total virial. The outer lying neighboring shells have been treated in a static lattice approximation (450 particles with a contribution in the order of 10% of the total energy). The rest is treated in a continuum static approximation with 1% contribution to the energy. It is worth mentioning that corrections of that kind, commonly used in condensed-matter simulations,[18] are important to make data, computed at constant pressure, quantitatively comparable to experiment. The total correction potential is computed at a reference volume V_0 and splits into two parts $v_{0,6}^{(\mathrm{cor})}, v_{0,12}^{(\mathrm{cor})}$. If the scale variable s changes, the corrections in potential change also and have to be considered in the Metropolis procedure [see Eq. (4)].

In most of the PIMC computations, we choose the Trotter number P between 4 and 16. During one MC step every bead and the center of mass of one chain make one trial move. The sequential update of all beads in a randomly chosen chain consists of random displacements in real space, with a maximum displacement chosen such that the resulting Metropolis acceptance ratio is about 30%. The number of equilibration steps is chosen to be bigger than $100P$. After relaxation data points were taken all $2P$ MC steps for averaging. At least 100 (independent) observations are made. Quantum limit is reached by applying Trotter scaling, see Sec. III.

III. FINITE-SIZE EFFECTS AT LOW TEMPERATURES

Only in the last decade[4] the PIMC method has been used to determine quantum contributions arising from the anharmonicity of realistic model potentials of solid matter. Already in previous work for convenience noble-gas solids have been chosen, because their interaction is known very accurately and its description, with a Lennard-Jones potential plus three-body corrections if necessary, is very easy. Bulk ^{4}He (Ref. 4) and linear chains of Lennard-Jones atoms have been investigated,[19,20] later a three-dimensional argon crystal was simulated[7,22] with a very powerful extension of PIMC, leading to the formulation of an effective "classical" potential. This approach is based on the assumption that any solid can be described in the harmonic approximation at zero temperature. This method however cannot be applied if anharmonicities already are important in the ground state.[22] It thus will be a challenge to this method to compute isotope effects in the lattice constant of rare gas solids, which are a consequence of anharmonicity in the ground state.

The question, whether the quantum limit has been reached within a finite Trotter decomposition, is discussed in nearly all PIMC simulation studies of condensed Lennard-Jones systems. Depending on the choice of the algorithm, the expectation value of the observable $\langle O\rangle = \mathrm{tr}\,[O\exp(-\beta H)]/\mathrm{tr}\,[\exp(-\beta H)]$ has a systematic error[23] $\delta\langle O\rangle$, with

$$\delta\langle O\rangle \propto P^{-2z}, z\epsilon N \tag{7}$$

if the approximant in the density matrix is chosen Hermitian, as in the primitive form where $z = 1$. This knowledge about the systematic error can be used to extrapolate to the quantum limit or one can argue that the quantum limit is already reached within statistical uncertainties, if P is large enough.

If thermodynamic properties are governed by long-wave excitations, as in noble-gas solids at low temperature by phonons, an additional scaling has to be carried out. The finite particle number N and Born–von Karman boundary conditions are leading to a discretization of energy spectra. In the quantum case this leads to a dependence of thermodynamic functions on the system size, while thermodynamic functions of classical systems do not change at all in the harmonic approximation.

A classical solid always becomes harmonic when the temperature tends to zero, provided that it is mechanically stable. The computed ground state energy only depends on the cutoff radius and thus does not change anymore when the simulation box is bigger than (twice) the cutoff radius. The specific heat is given by the law of Dulong-Petit. Thermodynamic functions thus do not depend on the system size when the temperature is low.

In the quantum case every elementary excitation with wave number k has its proper contribution to the thermal energy, specific heat, and so on. Let us call this contribution $f(k)$. A macroscopic observable quantity O is then given by the integration over all k values in the first Brillouin zone. This integration can be carried out by choosing points k_i in the first Brillouin zone and d-dimensional Taylor expanding $f(k)$ at k_i. The choice of the complete set of $\{k_i\}$ is given by the simulation box geometry and the periodic boundary conditions. In cubic geometry the k spacing in direction of the main axes is constant ($2\Delta k$). The resulting leading order terms are given by the first even order terms in the Taylor expansion, the odd terms vanish after integration, see below. We schematically sketch the integration over the phonon branch in the $(1,0,0)$ direction, where we choose $k_i = 2i\Delta k$:

$$\int_{-k_{\max}}^{k_{\max}} dk f(k) = \sum_{\{i\}} \int_{k_i-\Delta k}^{k_i+\Delta k} dk \sum_{l=0}^{\infty} \frac{1}{l!} f^{(l)}(k_i)(k-k_i)^l$$
$$= \sum_{\{i\}} 2 \sum_{l=0}^{\infty} f^{(2l)}(k_i) \frac{\Delta k^{(2l+1)}}{(2l+1)!}, \quad (8)$$

where $f^{(l)}(k_i)$ denotes the lth derivative of $f(k)$ at (k_i). In a computer simulation observables are measured in real space. If their measurements would be transformed into the momenta space, the corresponding terms of these measurements are those with $l = 0$ in Eq. (8), thus the two leading errors of discretization $\varepsilon_1, \varepsilon_2$ are

$$\varepsilon_1(\Delta k) = 2\frac{\Delta k^3}{3!} \sum_{\{i\}} f^{(2)}(k_i), \quad (9a)$$

$$\varepsilon_2(\Delta k) = 2\frac{\Delta k^5}{5!} \sum_{\{i\}} f^{(4)}(k_i). \quad (9b)$$

The finite size of the simulation box would lead to a finite Δk in Eqs. (8) and (9). Due to the translational symmetry in k space, the numerical integration from $k_i - \Delta k$ to $k_i + \Delta k$ in Eq. (8), resulting in a smaller systematic error than an integration from k_i to $k_i + 2\Delta k$, is justified automatically. The exact integral of any $f^{(l>0)}$ over one branch is zero because of the translational symmetry in k space, but not the discretized sum. The order of magnitude of the total sum cannot be bigger than one, which we assume to be the case. In the full d-dimensional integration the leading order discretization errors are still $\propto \Delta k^3$ and Δk^5. If we express the proportionality of Δk with respect to the particle number N in a d-dimensional space,

$$\Delta k \propto N^{-1/d}, \quad (10)$$

and insert this into Eq. (9) we obtain

$$\varepsilon_1(N^{-1/d}) \propto N^{-3/d}, \quad (11a)$$

$$\varepsilon_2(N^{-1/d}) \propto N^{-5/d}. \quad (11b)$$

Equation (11) gives an instruction how to scale computed observables with finite N to $N \to \infty$, when k is a good quantum number. We apply this scaling method to a three-dimensional fcc-Ar solid, defined in the computer, with periodic boundary conditions. The Lennard-Jones potential is treated in the harmonic approximation, thus all allowed values of k are good quantum numbers. The eigenenergies $E(k)$ can then be computed and from them the partition function $Q(\beta) = \sum_k \exp[-\beta E(k)]$ at any temperature follows. It depends on the number of atoms, which k values are allowed, and in Fig. 1 we present the internal energy $u_N(T) = -(1/N)[\partial \ln Q(\beta)/\partial\beta]$ and in Fig. 2 the specific heat $c_V(T) = \partial u_N(T)/\partial T$ at a given temperature and density for different particle numbers $N_l = 4l^3$, $l = 3, 4, \ldots, 9$. The computed data are fitted according to Eq. (11). The corrections to energy are only in the first order ϵ_1. For the accurate description of the specific heat data, see Fig. 2, we also need the term $\epsilon_2 \propto N^{-5/3}$.

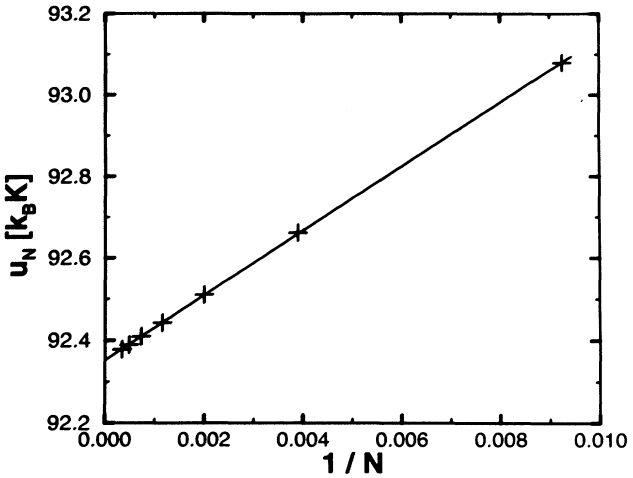

FIG. 1. Scaling plot for the internal energy u_N of solid ^{40}Ar in the harmonic approximation at $T = 4$ K vs inverse particle number (symbols). The line is a fit according to Eq. (11a).

Of course higher order corrections may be necessary if the temperature is very low (if one assumes that N has an upper bound in practical use of computers). Consider a typical dispersion relation $\omega(k)$ in the form of

$$\omega(k) = \frac{v}{\nu} \left(\frac{k}{k_D}\right)^{\nu}. \quad (12)$$

For phonons $\nu = 1$ and in the Debye model k_D proportional to the Debye temperature T_D, v corresponds to the group velocity. (For ferromagnetic magnons $\nu = 2$.)

In any textbook on solid state physics, that kind of

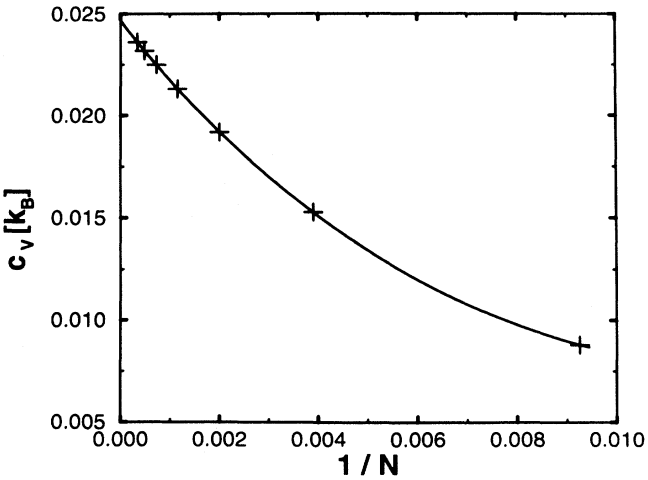

FIG. 2. Scaling plot for the specific heat c_V of solid ^{40}Ar in the harmonic approximation at $T = 4$ K vs inverse particle number (symbols). The line is a fit according to Eqs. (11a) and (11b).

dispersion relation for (boson) excitations is discussed. The following low temperature specific heat $c_V(T)$ is obtained:

$$c_V(T) \propto \left(\frac{T}{T_D}\right)^{d/\nu}, \quad T \to 0. \tag{13}$$

In the computer solid the possible k values are discretized, due to the finite-size according to Eq. (10) and this in turn leads with Eq. (12) to a lowest nonzero excitation frequency $\omega_{\min}$:

$$\omega_{\min} \propto N^{-\nu/d}. \tag{14}$$

The computer solid thus begins to exhibit a qualitatively different specific heat, when the temperature is smaller than $\hbar\omega_{\min}/k_B T$, because internal energy minus ground state energy vanishes exponentially fast $\propto \exp(-\hbar\omega_{\min}/k_B T)$. It is evident that size scaling in these temperature regimes is strongly recommended in order to find the right thermodynamic behavior. This can bee seen in Fig. 3, where the specific heat as a function of temperature is plotted for different system sizes. The smaller the system is, the more rapid is the decay of the specific heat with the temperature. It is nearly impossible to find a temperature region with specific heat $c_V \propto T^3$ for systems with less than 500 particles. Note that there are still many simulations in the recent literature where due to the use of complicated potentials appropriate for real materials or other technical reasons particle numbers less than 10^3 are used, and hence one must expect limitations of this sort to occur in such work.

Up to now, we discussed Trotter scaling in the infinite-size limit or size scaling in the infinite Trotter number limit. Of course, in general, one can neither do practical calculations in the quantum limit if no approximations are made, nor install an infinite number of particles in a simulation box. Using Eqs. (7) and (11), an observable $O\left(N^{-3/d}, P^{-2z}\right)$ with leading errors of order $N^{-3/d}$ due to finite N and leading errors of order P^{-2z} due to finite P can be written formally:

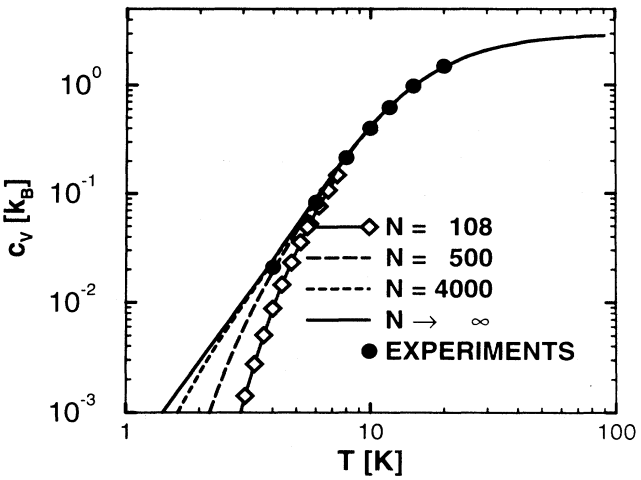

FIG. 3. The specific heat c_V of solid ^{40}Ar in the harmonic approximation, as a function of temperature, for different system sizes: $N = 108, 500, 4000$ and in the infinite particle number limit. Some experimental points (Ref. 21) are shown for comparison.

$$\langle O\left(N^{-3/d}, P^{-2z}\right)\rangle = \langle O(0,0)\rangle + \left[\frac{\partial\langle O\left(N^{-3/d}, 0\right)\rangle}{\partial(N^{-3/d})}\right]_{N\to\infty} N^{-3/d} + \left[\frac{\partial\langle O\left(0, P^{-2z}\right)\rangle}{\partial(P^{-2z})}\right]_{P\to\infty} P^{-2z} + \mathcal{O}\left(P^{-4z}, P^{-2z}N^{-3/d}, N^{-5/d}\right). \tag{15}$$

If one makes a scaling plot, one computes observables for a set of Trotter numbers P_i or a set of particle numbers N_i, with $i = 1, 2, \ldots, i_{\max}$, then the observables are plotted against P^{-2z} or $N^{-3/d}$ and extrapolated to $P \to \infty$ or $N \to \infty$. It thus would be highly desirable to make this extrapolation in one step. To do this one would have to choose:

$$\left(\frac{P_1}{P_i}\right)^{2z} = \left(\frac{N_1}{N_i}\right)^{3/d}. \tag{16}$$

Unfortunately, it is nearly impossible to find an adequate set of integers P_i, N_i, which fulfill this condition. Nevertheless one can always find a pair of integers $N_{\max}, P_{\max}$. If the particle number lowered now, one has to carry out two simulations with different Trotter numbers and interpolate between them. This procedure will be less expensive in CPU time compared to carrying out the full extrapolation to the quantum limit, above all an interpolation between Trotter numbers is much less risky than an extrapolation to infinite Trotter number. After a proper choice of such an integer pair $N_{\max}, P_{\max}$ interpolations are not required at high Trotter numbers and high particle numbers, but only less expensive interpolations at lower total numbers of beads. In a set of computations, where N_i and P_i are chosen according to Eq. (16) the leading error ϵ_1 is proportional to P_i^{-2z} and $N_i^{-3/d}$, respectively,

$$\epsilon_1(i) \propto P_i^{-2z} \propto N_i^{-3/d}. \tag{17}$$

Of course the proportionality constant depends on temperature, pressure and so on. Before we apply this combined Trotter and size scaling to an Ar crystal, we check to which extent the harmonic approximation is valid and we investigate the influence of finite Trotter number on

the internal energy. The Debye temperature T_D is in the order of 100 K. As can be seen in Fig. 4, $P = 4$ describes well the internal energy down to 30 K, the $P = 16$ curve down to 10 K. The classical limit is reached at temperatures around T_D. Below the discussed temperatures the curves begin to show qualitative deviations from the quantum limit behavior in the harmonic approximation. It can be seen furthermore that the expectation values of potential energy are always smaller than those of the kinetic energy, which are quite close to the predictions of the harmonic approximation. For $T \to 0$ we detect a relative difference between $T_{\rm kin}$ and $V_{\rm pot}$ of 0.07, see below in this section. Thus any calculated results, being much closer to experiment than 0.07 would imply an overinterpretation of model potential parameters. In terms of perturbation theory the deviations from the harmonic approximation are very easy to understand. Potential energy already changes in the first order of perturbation, while the kinetic energy can only change in second and higher order.

We now apply the combined size and Trotter scaling to the internal energy at T =4 K. From Fig. 4 we learn that $P \geq 16$ should already yield good results, from Fig. 3 we learn that $N = 500$ gives good values of specific heat in this temperature region. We thus choose one pair of integers for the scaling plot $(P, N) = (64, 500)$. Note that this choice corresponds to a simulation effort of 32 000 particles in a purely classical system, which is not a trivial effort. The other pairs had been chosen with $N = 4l^3$ with $l = 4, 6, 7, 8, 9$, and P according to Eq. (16). In Fig. 5 we show the combined scaling plot for internal energy as a function of N^{-1}. The scaling plot in the full quantum limit is also shown for comparison and both curves intersect at $N \to \infty$.

In order to quantify the anharmonicity effects at zero temperature we studied the relative difference between

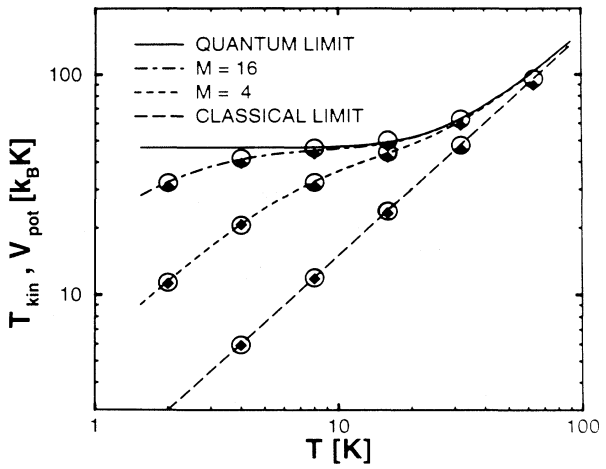

FIG. 4. Kinetic and potential energies of ^{40}Ar as a function of temperature, for different Trotter dimensions $P = 1$ (classical), 4, 16 and in the quantum limit ($P \to \infty$) in the harmonic approximation (lines) and simulated results (symbols). Circles correspond to kinetic energy ($T_{\rm kin}$), diamonds to potential energy ($V_{\rm pot}$). The system size is $N = 256$, error bars are much smaller than symbol sizes.

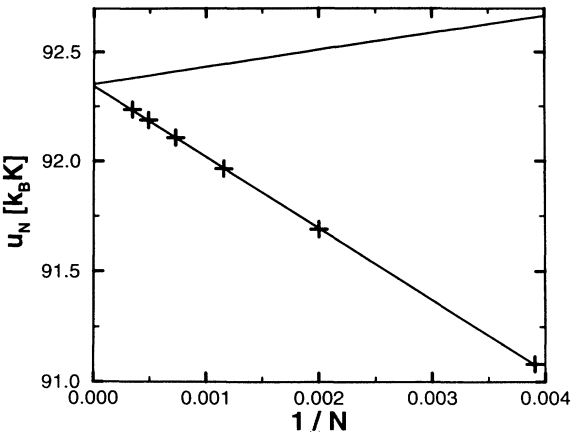

FIG. 5. Internal energy u_N as a function of inverse particle number in the harmonic approximation. The upper curve corresponds to the full quantum limit. Symbols show results of the harmonic approximation [see text and Eq. (16)], the lower curve is a scaling plot according to Eq. (17).

$T_{\rm kin}$ and $V_{\rm pot}$ by the anharmonicity parameter $\delta := 2(T_{\rm kin} - V_{\rm pot})/(T_{\rm kin} + V_{\rm pot})$. The limit $\lim_{T\to 0} \delta(T)$ is obtained by extrapolation of finite temperature data, keeping $P = (32K/T)^2$. The error in the primitive algorithm decays with[23,3] $(PT)^{-2}$, thus with our choice of P and T the systematic error vanishes proportional to T^2. Thermal excitations vanish still faster due to the small specific heat [see Fig. 3, Eq. (13)]. We thus can extrapolate δ, see Table I, quadratically to zero temperature. The value of the classical simulation ($P = 1$) was excluded from the extrapolation.

At the end of this section we want to emphasize that the combined size and Trotter scaling proposed in this paper is applicable to periodic systems. The concrete form of Eqs. (15)–(17) therefore cannot be applied directly to superfluid liquids or even less to disordered solids. Nevertheless, finite-size effects as mentioned above should also occur in that kind of system and a careful analysis will also be necessary in order to determine by simulation how specific heat or expansion coefficients are tending to zero with $T \to 0$.

IV. SIMULATION OF ISOTOPE EFFECTS IN LATTICE CONSTANTS

In the first application of PIMC to quantum many-body systems,[4] it was shown that spatial correlation

TABLE I. Anharmonicity parameter δ for ^{40}Ar at different temperatures. The value at $T = 0$ K is obtained by extrapolation, see text.

T (K)	P	100 $\times\delta$
32	1	3.74
16	4	5.40
8	16	6.37
4	64	6.69
0	∞	6.75

functions in the fluid and solid phases of ^{4}He can be obtained with high accuracy. Quantum nature of particles can lead to different isotope effects. The melting curves of ^{3}He and ^{4}He differ slightly, while the classical melting curve does not depend on the masses of the given species. These effects have been computed in good agreement with experiment within PIMC simulations.[8,9] Solid neon also exhibits an isotope effect in the lattice constant, which has not yet been investigated within a PIMC approach. We carried out a PIMC simulation at zero pressure for ^{20}Ne and ^{22}Ne at different temperatures.

Based on a Trotter scaling plot analysis, it turns out that convergence for the lattice constant is reached as fast as for other thermodynamic functions like energy and specific heat, but due to the small fluctuations of volume, lattice constants can be detected with a very high precision. In Fig. 6 we show such a scaling plot for both investigated neon species at a temperature $T = 16$ K, which is smaller than but in the order of the Debye temperature. Trotter scaling can be applied at this temperature, with Trotter numbers $P = 4, 6, 8, 10$. We carried out such a scaling (plot) with suitable Trotter numbers for temperatures $T = 8, 10, 12, 16, 18, 20, 22$ K. In order to avoid the smallest systematic errors, we always chose the same Trotter numbers and the same number of equilibration and observation MC steps for both isotopes at a given temperature.

In Fig. 7 we show the obtained expectation values of the lattice constant as a function of temperature and we also present for comparison experimental data and classical data with and without correction potentials (see Sec. II). The qualitative behavior of experiment and PIMC simulation is quite similar. We have not been interested in optimizing the potential in order to achieve perfect agreement with the experimental data and present this comparison just as an illustrative example. We only want to remark that the Lennard-Jones parameter σ used in the literature is chosen between[5] 2.75 and[6] 2.79 Å, with a relative difference of 2%. We use the smallest value 2.75 Å and we obtain a lattice constant 1% smaller than the experimental one. It thus would be easy to obtain still better agreement, also with potential parameters within the usual range. We note again that in the classical simulations no mass effects are present resulting in the same lattice constants for ^{20}Ne and ^{22}Ne.

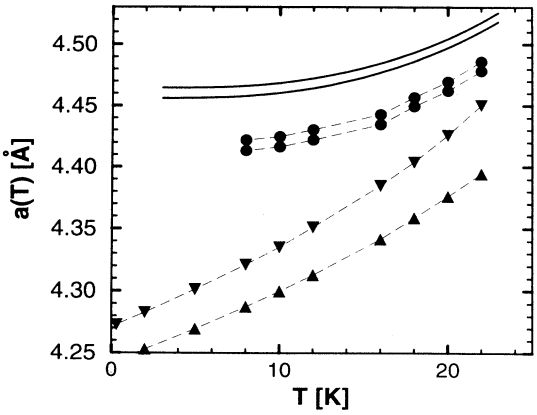

FIG. 7. Lattice constant a of ^{20}Ne and ^{22}Ne: experimental data (full lines), PIMC results (circles); upper curves: ^{20}Ne, lower curves: ^{22}Ne. Classical MC data with correction potential (triangles up) and without correction potential (triangles down). Error bars are smaller than symbol sizes, dashed lines are drawn to guide the eye.

Of course the hardest test is to detect (relative) differences in the lattice constant and we define the relative difference in the lattice constant $\chi = ({}^{20}a - {}^{22}a)/{}^{22}a$. In Fig. 8 we compare the computed results with experimental data. All points agree within statistical error and a little offset, which may have its origin in the three-body forces or in the choice of Lennard-Jones parameters. At temperatures below ≈ 20 K, χ decreases with increasing temperature due to the approach to the classical high temperature limit ($\chi = 0$). At higher temperatures χ in-

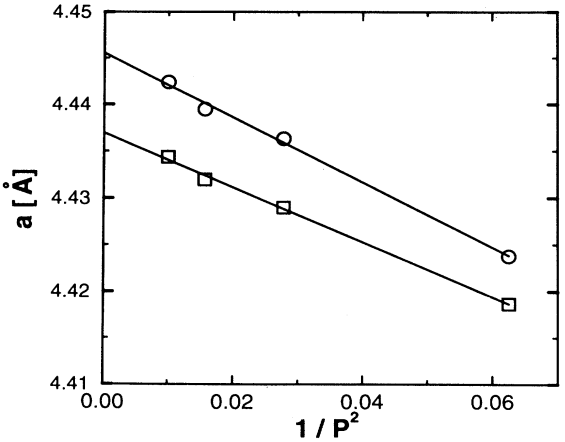

FIG. 6. Trotter scaling plot for the lattice constant a of solid neon. The upper curve corresponds to ^{20}Ne, the lower curve to ^{22}Ne at $T = 16$ K. Symbols: PIMC results, error bars are smaller than symbol sizes.

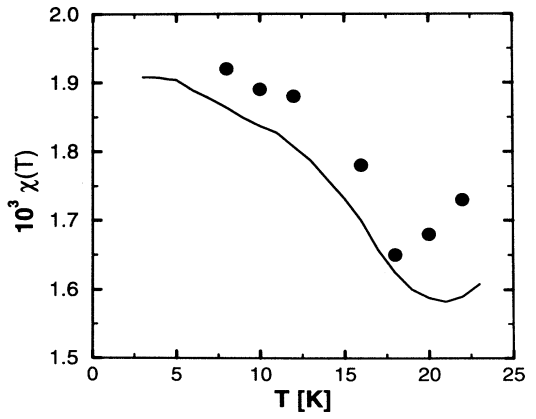

FIG. 8. Relative difference χ of the lattice constants of ^{20}Ne and ^{22}Ne as a function of temperature. Lines are experimental values (Ref. 11), symbols are PIMC results, the error bars of the $10^3\chi(T)$ data values are about ± 0.03.

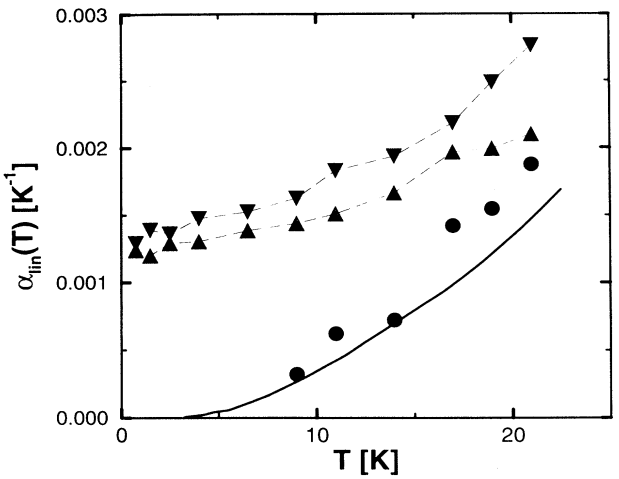

FIG. 9. Linear thermal expansion coefficient α_{lin} of ^{20}Ne as a function of temperature. Lines correspond to experimental values (Ref. 11), circles to PIMC data, triangles to classical MC data with (triangles up) and without (triangles down) correction potentials, the error bars of the $\alpha_{lin}(T)$ data values are about ± 0.0002. Dashed lines are drawn to guide the eye.

creases with temperature in agreement with experimental findings. This increase in χ may be attributed to the approach of the temperature to the melting temperature, which is lower for ^{20}Ne resulting in an increasing lattice constant for ^{20}Ne. We note that the resolution is of order 0.1% of the lattice constant ($\approx$ 10 fm).

Another observable of interest is the relative thermal (linear) expansion coefficient $\alpha_{lin} = [da(T)/dT]/a$ (see Fig. 9). This computed observable also agrees within a little offset of about 15% with experimental data. It is worth mentioning that this offset would be much bigger if the static correction potentials described in Sec. II B would not have been considered. In order to prove this, we insert classical MC data with and without correction potentials. At temperatures higher than 20 K the influence of the potential corrections on α_{lin} becomes more important than that of the quantum nature. Below 20 K the difference between the thermal freezing of a real quantum solid and a classical solid can also be seen in Fig. 9. The interpretation can easily be done in terms of Grüneisen theory. The quantum phonon occupation numbers no longer change drastically at temperatures smaller than T_D, thus anharmonicity effects attributed to phonons, like thermal expansion, also do not change any longer. In the classical case the amplitudes of sound excitations are not discretized and α_{lin} does not tend to zero at very low temperatures. The harmonic approximation only is fulfilled in the sense that potential and kinetic energy with respect to the classical ground state are equal.

V. CONCLUSION AND DISCUSSION

Path-integral Monte Carlo is a suitable method to simulate low temperature vibrational dynamics of solids. The lattice constant and associated structural properties can clearly be resolved. This was shown by computing the isotope shift in the lattice constant of ^{20}Ne and ^{22}Ne with a very high accuracy. The thermal expansion coefficient has been computed as well in good agreement with available experimental data.

At very low temperatures however much effort has to be done in order to avoid discretization effects of phonon spectra, resulting in an artificial fast decrease of specific heat with decreasing temperature. We have proposed a combined Trotter and size scaling, in order to reduce strongly the required computational effort if size dependence is to be eliminated. Nevertheless better approximants as in the primitive algorithm are necessary in order to be able to compute "critical" exponents describing how the specific heat vanishes as the temperature goes to zero. Of course their detection is very hard for pure crystals, since this exponent only can be measured at temperatures small in comparison to the Debye temperature, e.g., at $T = 0.05T_D$.

Crystals containing a few impurities, or heavily disturbed solids such as mixtures, orientational glasses, and so on show anomalies in the specific heat which should be more easy to detect, hence there exists an amount of specific heat bigger than the part attributed to the phonon spectra of the pure system. This amount of specific heat should suffer less from statistical noise of the energy estimator, which always is on the order of the statistical noise of a classical simulation, since any straightforward PIMC method uses quasiclassical moves of single beads and total chains, independent of the formulation of the high temperature density matrix. PIMC simulation thus could illuminate the understanding of thermal and structural anomalies of this kind of condensed matter.

ACKNOWLEDGMENTS

This research was carried out in the framework of the Sonderforschungsbereich 262 der Deutschen Forschungsgemeinschaft. P.N. thanks the DFG for financial support (Heisenberg foundation). The computations were carried out on the CRAY YMP of the HLRZ at Jülich.

[1] K.E. Schmidt and D.M. Ceperley, in *The Monte Carlo Method in Condensed Matter Physics*, Topics in Appl. Phys. Vol. 71, edited by K. Binder (Springer, Berlin, 1992).

[2] *Quantum Simulation of Condensed Matter Phenomena*, Proceedings on an International Workshop, edited by J.D. Doll and J.E. Gubernatis (World Scientific, Singapore, 1990).

[3] *Quantum Monte Carlo Methods in Equilibrium and Nonequilibrium Systems*, edited by M. Suzuki, Springer Series in Solid State Sciences Vol. 74 (Springer, Berlin, 1987).

[4] E.L. Pollock and D.M. Ceperley, Phys. Rev. B **30**, 2555 (1984).
[5] D. Thirumalai, Randall W. Hall, and B.J. Berne, J. Chem. Phys. **81**, 2523 (1984).
[6] J.J. Morales and K. Singer, Mol. Phys. **73**, 873 (1991).
[7] Alessandro Cuccoli, Valerio Tognetti, and Ruggero Vaia, Phys. Rev. **B 45**, 2088 (1992)
[8] Jean-Louis Barrat, Paul Loubeyre, and Michael L. Klein, J. Chem. Phys. **90**, 5644 (1989)
[9] M. Boninsegni, C. Pierleoni, and D.M. Ceperley, Phys. Rev. Lett. **72**, 1854 (1994).
[10] K.S. Schweizer, R.M. Stratt, D. Chandler, and P.G. Wolynes, J. Chem. Phys. **75**, 1347 (1981).
[11] D.N. Batchelder, D.L. Losee, and R.O. Simmons, Phys. Rev. **173**, 873 (1968).
[12] R.P. Feynman and A.R. Hibbs, *Quantum Mechanics and Path Integrals* (McGraw-Hill, New York, 1965).
[13] D.M. Ceperley and E.L. Pollock, in *Monte Carlo Method in Theoretical Physics*, edited by S. Caracciolo and A. Fabrocini (ETS, Pisa, 1991).
[14] D.C. Chandler and P.G. Wolynes, J. Chem. Phys. **74**, 4078 (1981).
[15] M.F. Herman, E.J. Bruskin, and B.J. Berne, J. Chem. Phys. **76**, 5150 (1982).
[16] The used Lennard-Jones potential parameters and masses are $\epsilon_{\mathrm{ArAr}} = 121$ K, $\sigma_{\mathrm{ArAr}} = 3.405$ Å, $m_{\mathrm{Ar}} = 40$ amu, $\epsilon_{\mathrm{NeNe}} = 35.8$ K, $\sigma_{\mathrm{NeNe}} = 2.75$ Å, ${}^{20}m_{\mathrm{Ne}} = 20$ amu, ${}^{22}m_{\mathrm{Ne}} = 22$ amu.
[17] C. Chakravarty, J. Chem. Phys. **99**, 8038 (1993).
[18] M.P. Allen and D.J. Tildesley, *Computer Simulation of Liquids* (Claredon, Oxford, 1987).
[19] A.R. Mc Gurn, P. Ryan, A.A. Maradudin, and R.F. Wallis, Phys. Rev. **B 40**, 2407 (1989).
[20] A. Cuccoli, V. Tognetti, and R. Vaia, Phys. Rev. B **41**, 9588 (1990).
[21] O.G. Peterson, D.N. Batchelder, and R.O. Simmons, Phys. Rev. **150**, 703 (1966).
[22] A. Cuccoli, A. Macchi, V. Tognetti, and R. Vaia, Phys. Rev. **B 47**, 14923 (1993).
[23] R.M. Fye, J. Stat. Phys. **43**, 827 (1986).